Probing ultrafast photochemical mechanisms of molecular and heterogenized rhodium bipyridine photocatalyst

Quentin Périnnet[a], Ashta C. Ghosh[b], Jérôme Canivet[b], Florian Wisser[b,c], Vincent De-Waele[a*]

[a] Univ. Lille, CNRS, UMR 8516, LASIRE-Laboratoire de Spectroscopie pour les Interactions, la Réactivité et l'Environnement, Lille, 59000, France
[b] Université Claude Bernard Lyon 1, CNRS, IRCELYON - UMR 5256, 2 Avenue Albert Einstein, 69626 Villeurbanne Cedex, France
[c] Erlangen Center for Interface Research and Catalysis, Friedrich-Alexander-Universität Erlangen-Nürnberg, Egerlandstraße 3, 91058 Erlangen, Germany

*vincent.de-waele@univ-lille.fr

Abstract

Molecular and heterogenized rhodium bipyridine (Bpy) complexes are highly active and selective for the carbon dioxide photoreduction into formic acid using visible light as sole energy source. The excited state of the molecular 5,5'-di(pyren-1-yl)-2,2'-bipyridine **Pyr_2Bpy** and of the corresponding conjugated microporous polymer **PyrBpy-CMP**, envisioned as macroligand, as well as of their organometallic complexes with pentamethylcyclopentadienyl (Cp*) rhodium **$[Pyr_2Bpy]Cp^*RhCl_2$** and **Cp*Rh@PyrBpy-CMP** have been investigated by femtosecond UV-vis transient absorption spectroscopy. In both polymers **PyrBpy-CMP** and **Cp*Rh@PyrBpy-CMP** the fs measurements reveal the formation of a broad excited state absorptions bands decaying in the sub-ns time scale. For **Cp*Rh@PyrBpy-CMP** , the ultrafast energy transfer from the framework to the catalytic centres is demonstrated. **Pyr_2Bpy** and **$[Pyr_2Bpy]Cp^*RhCl_2$** have been studied as model molecular building blocks of the CMP. The results show the participation of a mesomeric intramolecular charge transfer (MICT) state and of a twisted intramolecular charge transfer state (TICT) stabilized by the torsion of the pyrene and bipyridine moiety, that are then converted into ligand to metal charge transfer states (LMCT) in **$[Pyr_2Bpy]Cp^*RhCl_2$**. The photophysical parameters determined for the molecular compounds were applied to calculate the Förster Resonance Energy Transfer rate from the light-harvesting organic units to the heterogenized Rh metal centres. Finally, the role of the triethanolamine, a common sacrificial electron donor (SED) employed for the CO_2 reduction, as an efficient quencher of the excited states of the Pyr_2Bpy is demonstrated. This quenching reaction is expected to occur for a wide range of organic and organo-metallic photocatalysts, and its consequences on the reduction of the photoconversion yield are certainly underestimated for most of the applications.

Keywords: ultrafast transient spectroscopy, light-harvesting, photochemistry, Porous Organic Polymers, Rhodium, Photocatalysis, Carbon Dioxide

Introduction

The site-isolation of organometallics complexes in porous organic frameworks has emerged as a promising route to design artificial supramolecular assemblies for photocatalysis[1–3]. In these photoactive materials, the porous framework made of electron-rich organics linkers constitutes a large antenna[4–10] carrying out the absorptions of the photons and the subsequent conversion and transfer of the energy to the metal centres in charge of the catalytic activity.

One of the challenges for applying this strategy to the development of efficient photocatalyst is to optimise the synergy between the cooperative effects along the organic framework [3,10–13]and the single-site activation and reactivity of the metal centres. The main bottleneck is the collection the light on large area around the catalytic centre followed by an ultrafast and efficient energy transfer to achieve multiple electron injections on a short period of time.

Ultrafast time-resolved spectroscopy has been applied to resolve the formation of separated electron-hole pairs (e^--h^+) between linkers and metal centres in metal-organic-frameworks (MOFs). Douhal and co-worker[14,15] have shown that in Zr-naphtalene-dicarboxylate (Zr-NDC) MOFs the charge separation takes place within less than 200 fs, leading to the formation of electrons and holes localized on the Zr clusters and on the naphtalene linkers, respectively. The (e^--h^+) pairs can be engaged in one-electrons redox reactions. The analysis of the decays shows also that the electron-hole recombine radiatively with different lifetimes varying from the hundreds of ns to the µs time scale, suggesting the presence of heterogenous trapping environments in the materials. In additions, time-resolved measurements also revealed that the (e^--h^+) formation is in competition with the formation of excimers or energy transfer. The role of the topology of the MOFs framework in controlling these competitive pathways has also been evidenced for Zr-(*p*-benzoic acid)-pyrene MOF materials (NU-901, NU-1000)[16] and in MOF PCN-223, for which a hopping mechanism of energy transfer from the excited chromophores to N-protonated linkers acting as traps has been proposed.[17] The titanium-based MOF family MIL-125(Ti) have also attracted a lot of attention for solar fuel generation. The photocatalytic activity of the MIL-125(Ti) is due to a photoinduced electron transfer from the HOMO orbitals of the ligand into the LUMO orbitals localized on the Titanium-oxo clusters. The incorporation of amino (-NH_2) group in some of the ligand is shifting the absorption wavelength of the MOF to the visible spectral range and favour the stabilisation of the electron-hole pair, as it has been shown by transient UV-vis and MidIR femtosecond spectroscopy[18,19]. For MIL-125 derivatives, and MOFs in general, understanding the crucial influence on the ligand substituent on the photocatalytic activity[18,20–24] is of great importance to optimize the applications. Interestingly, by comparing the effect of triethanolamine (TEOA) and of methanol (MeOH) as hole scavengers for the photocatalytic HER process with MIL-125(Ti) and NH_2-MIL-125(Ti), Eder and co-workers[22] have shown that the charge stabilization on the amino group is not favourable to the hole scavenging by MeOH, while TEOA molecules degrade the MIL-125(Ti). These works illustrate the complex interplay between the different and often competitive primary photophysical and photochemical processes governing the electron-hole formation and reactivity in microporous photocatalysts. The properties of the excited states, the mode of energy transfer and of charge separation toward the metal centre vary finely with the nature and composition of the porous materials. Thus, there is still a pressing need for more systematic and in-depth investigation of these ultrafast processes to be carried out in line with the design of new and promising photocatalyst. The work reported hereafter aims to contribute to that field by focusing on the excited photochemistry of metal containing conjugated microporous polymers (CMP), a class of porous materials for which the application of the time-resolved spectroscopy is still quite limited compared to MOFs, despite their interest for photocatalysis applications[25–27].

CMP are amorphous materials, made by covalent bonding between aromatic organic monomers, with large specific surface area[28] and they can potentially exhibit electronic properties close to those of semiconducting materials. They can be furthermore combined with metal centres (M) dispersed through the porous framework to design photoactive catalysts. In order to conceptualize the mechanisms at play within these heterogenous materials as photocatalysts, two limiting cases have to be considered[29] that are, on one side, the π-conjugation is dominating and the photoactivation results from an interband optical transition generating an electron hole-pair (exciton) that diffuses quasi-freely along the framework with stabilized electron (at, or close to, the metal centre) and hole (at the organic framework) and on the other side, the photoexcitation result in localized molecular excited states and activation proceeds by energy transfer (Förster, Dexter), and charge transfer, including the competition with the formation of exciplex species, as reported for MOFs. The photoinduced behaviour of M@CMP hybrids might be envisioned as a subtle mixture of these mechanisms, depending on the framework composition and metal binding, but also on the polymer topology (chain length and entanglement).

Recently, the electrocatalytically active Rh complexes has been unveiled to be efficient in visible light assisted CO_2 reduction in solution and heterogenized within MOF[30] . Extending this strategy of single-site immobilization of the catalyst within a porous framework[2,31-34], the development of bipyridine-based porous organic polymers as platforms for the heterogenization of pentamethylcyclopentadienyl rhodium (**Cp*Rh**) catalytic species showing notably remarkable photocatalytic performances in the CO_2 reduction to formic acid has been reported.[35] In these photocatalysts, the pyrene-bipyridine (**PyrBpy**) or perylene-bipyridine (**PerBpy**) moieties constitutes a photosensitive conjugated macroligand that can absorb the photons below 450 nm. Time-resolved emission spectroscopy has revealed that in presence of **Cp*Rh** linked to the **PyrBpy-CMP** or **PerBpy-CMP** framework as porous macroligand, the excited state formed by photoexcitation at 400 nm is quenched within a few tens to hundreds of picoseconds[35] featuring the ultrafast conversion between the excited stated state of the organic linkers to the activated metal centres. Quantum chemical calculations have been performed on a model [(5,5'-di(pyren-1-yl)-2,2'-bipyridine)(pentamethyl-cyclopentadienyl)rhodium] dichloride coordination complex, (hereafter **Cp*Rh@Pyr$_2$Bpy**) and determined the ligand-to-metal charge transfer (LMCT) character of the exited state triggering the catalytic activity of the rhodium metal centre[35]. The transient chemical species involved in the earliest stages of the CO_2 photoreduction by **Cp*Rh@Pyr$_2$Bpy-CMP** and **Cp*Rh@Per$_2$Bpy-CMP** microporous polymers have not been so far experimentally characterized.

The ultrafast time-resolved spectroscopy in the fs-ps time scale is a method of choice to characterize the initial charge separation and transfer processes governing the photochemical activity of the MOF materials.[14,15,36] Here we are reporting femtosecond UV-Vis transient absorption investigations of the excited states of the **Pyr$_2$Bpy** molecular ligand, of the **Cp*Rh@Pyr$_2$Bpy** complex**,** as model building block of the pyrene-bipyridine conjugated microporous polymer (**PyrBpy-CMP**) and of its corresponding Rh metallated catalysts **Cp*Rh@PyrBpyCMP**, respectively. The investigated compounds are shown in **Scheme 1**. The experiments were notably carried-out in acetonitrile:triethanolamine solution to elucidate the reaction between the excited states of the different compounds and the amine under the same reactive conditions of ref. [35]. These pump-probe measurements have been completed by steady state absorption and emission spectroscopy and by time-resolved emission measurements.

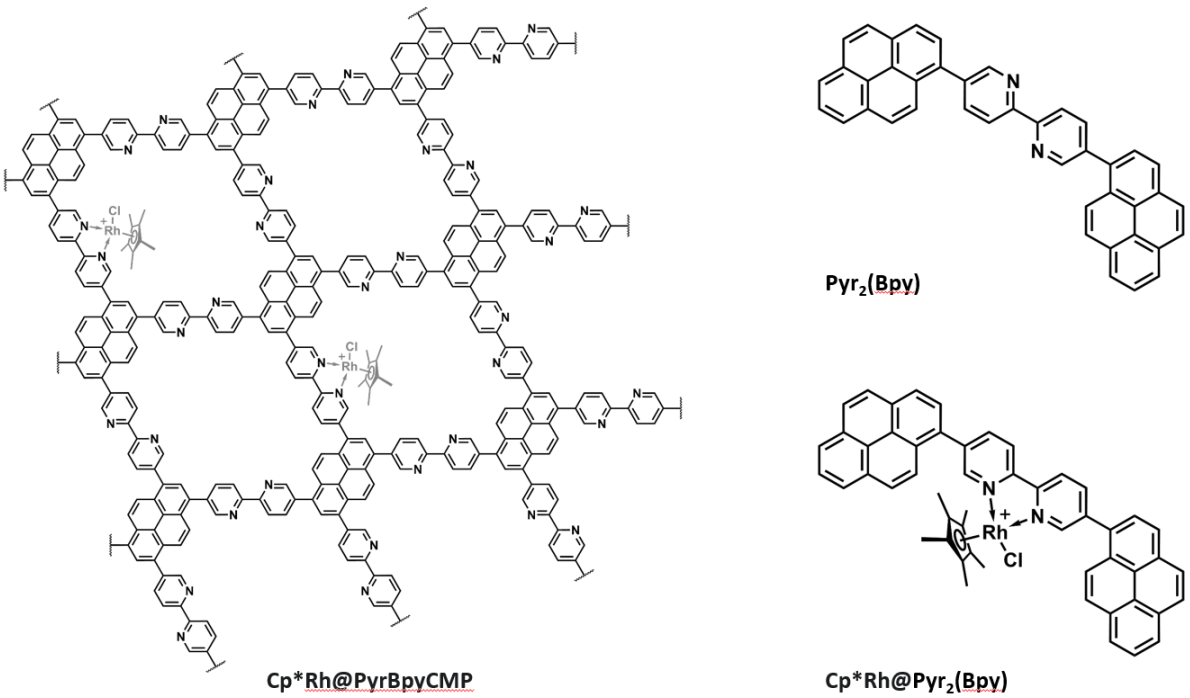

Scheme 1: Supramolecular assembly of the pyrene and of the bipyridine molecules forming the porous conjugated polymer (CMP). The drawing of the molecular compounds and of the porous CMP are only for illustration purpose; they do not aim to be a model of the structure of the polymer.

1. Experimental part

1.1. Chemicals and materials

DMF (anhydrous, 99.8 %), DMSO (anhydrous, ≥99.9 %), $Pd(PPh_3)_4$ (99.9 %), $Pd(dppf)Cl_2$, pentamethylcyclopentadienylrhodium(III) chloride dimer, potassium acetate (99.98 %), potassium carbonate (99 %), pyrene-1-ylboronic acid (>95 %), toluene (anhydrous, 99.8 %), were purchased from Sigma Aldrich. Acetonitrile (HPLC grade) was purchased from VWR, bis(binacolato)diborane (99 %), 5,5'-dibromo-2,2'-bipyridine (96 %) and 1,3,6,8-tetrabromopyrene (98 %) from TCI. Deuterated solvents were purchased from euriso-top. For the UV-vis steady state and transient spectroscopy measurements, Acetonitrile (Spectrophotometric grade, 99.7+%) from Alfa Aesar, THF (anhydrous, 99.8%), Propionitrile (GC Grade 99%), Butyronitrile (GC Grade, 99%) and Triethanolamine (TEOA, 99%) from Sigma-Aldrich were used.

Liquid NMR spectra were recorded on a Bruker Ascend 400 spectrometer (9.4 T, ^1H at 400.13 MHz, ^{13}C at 100.61 MHz). The spectra were referenced against the residual solvent signal.

1.2. Molecules and materials preparation

5,5'-di(pyrene-1-yl)-2,2'-bipyridine **Pyr_2Bpy**

The synthesis was done according to a modified literature procedure[31]:

In a 500 ml 2-neck round-bottom flask equipped with a reflux condenser 1.0 g (3.86 mmol) pyrene-1-ylboronic acid, 593 mg (1.85 mmol) 5,5'-dibromo-2,2'-bipyridine and 810 mg (7.64 mmol) Na_2CO_3 were dissolved in 200 ml toluene and 50 ml H_2O. The bi-phasic mixture was deaerated by bubbling Ar through it and then 220 mg (190 µmol) $Pd(PPh_3)_4$ were added under a flow of Ar. The reaction mixture was heated to reflux for 3 d under exclusion of light. Then, the mixture was cooled to room temperature, the solid formed isolated by filtration and washed with H_2O and Et_2O (each 60 ml). Drying under vacuum at room temperature gave 5,5'-di(pyren-1-yl)-2,2'-bipyridine as green solid. Yield: 980 mg (1.76 mmol, 91 %).

^{1}H NMR: (400.13 MHz, CD_2Cl_2/CF_3COOD, 1 : 1, *V* : *V*): δ 9.43 (d, 2H, J=2 Hz), 9.17 (dd, 2H, J=8.5, 2.0 Hz), 8.93 (d, 2H, J=8.5 Hz), 8.49-8.15 (m, 18H).
^{13}C NMR: (100.61 MHz, CD_2Cl_2/CF_3COOD, 1 : 1, *V* : *V*): δ 148.7, 146.8, 144.9, 142.5, 134.3, 132.4, 131.7, 131.2, 130.6, 129,6, 128.3, 128.2, 128.0, 127.9, 127.8, 127.2, 127.0, 126.3, 126.0, 125.3, 122.6.

[(5,5'-di(pyren-1-yl)-2,2'-bipyridine)(pentamethyl-cyclopentadienyl)rhodium]dichloride
[Pyr_2Bpy]Cp*$RhCl_2$

The synthesis was done according to a modified literature procedure[34,38,40]:

In a 100 ml round bottom flask 56.1 mg (90 µmol) $[Cp^*RhCl_2]_2$ and 100 mg (180 µmol) 5,5'-di(pyrene-1-yl)-2,2'-bipyridine were dispersed in a mixture of 4 ml MeOH and 4 ml CH_2Cl_2 and stirred at 70 °C for 4 h during which time the colour changed to a clear yellowish brown. After cooling to RT 50 ml Et_2O were added to the reaction mixture in order to achieve complete precipitation. The yellow precipitate was removed by filtration, rinsed with Et_2O. Drying under vacuum at room temperature gave (5,5'-di(pyrene-1-yl)-2,2'-bipyridine)(pentamethyl-cyclopentadienyl)rhodium] dichloride as yellow solid. Yield: 110 mg (124.89 µmol, 70 %).

^{1}H NMR: (400.13 MHz, MeOH-d_4): δ 9.18 (s, 2H), 8.80 (d, 2H, J=8.1 Hz), 8.56 (d, 2H, J=8.1 Hz), 8.34-8.08 (m, 18H), 1.71 (s, 15H).
^{13}C NMR: (100.61 MHz, MeOH-d_4): δ 154.48, 153.67, 143.20, 142.92, 133.72, 132.85, 132.20, 131.54, 130.41, 129.94, 128.76, 128.36, 127.87, 127.43, 126.93, 126.43, 125.72, 125.13, 124.35, 99.16, 9.07.

1,3,6,8-tetrakis(4,4,5,5-tetramethyl-1,3,2-dioxaborolan-2-yl)pyrene

The synthesis was done according to a modified literature procedure[38]:
Inside a glovebox a flame-dried schlenk tube was charged with 1.009 g (1.91 mmol) tetrabromopyrene, 2.976 g (11.60 mmol) bis(pinacolato)diboron, 125.7 mg (0.17 mmol) $Pd(dppf)Cl_2$ and 1.164 g (11.86 mmol) KOAc. Outside the glovebox, 20 ml anhydrous DMSO were added, the reaction mixture deaerated by three freeze-pump-thaw cycles and heated to 80°C for 2 d. Then, the mixture was cooled to room temperature, the brownish suspension was poured into 500 ml H_2O. The precipitate was isolated by filtration, washed with water and dried. The crude product was dissolved in DCM, passed through a plug of Celite and the solvent evaporated. For further purification the product was suspended in 30 ml toluene and heated to reflux. After 30 min at reflux the suspension was filtered hot, and the product washed twice with 20 ml of hot toluene. Drying under reduced pressure gave 1,3,6,8-tetrakis(4,4,5,5-tetramethyl-1,3,2-dioxaborolan-2-yl)pyrene as off-white powder. Yield: 0.513 g (0.73 mmol, 38 %)

^{1}H NMR: (400.13 MHz, $CDCl_3$): δ 9.16 (s, 4H), 8.99 (s, 2H), 1.50 (s, 48H).

^{13}C NMR: (100.61 MHz, $CDCl_3$): δ 141.32, 137.97, 129.42, 123.98, 83.82, 25.09.

PyrBpyCMP

The synthesis was done according to a literature procedure[35]:
Under Ar 124.8 mg (0.173 mmol) 1,3,6,8-tetrakis(4,4,5,5-tetramethyl-1,3,2-dioxaborolan-2-yl)pyrene, 111.2 mg (0.347 mmol) 5,5'-dibromo-2,2'-bipyridine, 6.4 mg (5.5 µmol) $Pd(PPh_3)_4$ and 147.4 mg (1.06 mmol) K_2CO_3 were dispersed in 7.5 ml DMF and 1.5 ml H_2O in a Schlenk tube. The reaction mixture was degassed by three freeze-pump-thaw cycles and heated to 150°C for 3 d. After the mixture had been cooled to room temperature, the polymer was poured into 1 N HCl, isolated by filtration and washed with water and MeOH. Further purification was performed by Soxhlet extraction for 2 d using THF and $CHCl_3$ for 1 d each. After drying under reduced pressure PyrBpyCMP was obtained as a yellow solid. Typical yield: 81.2 mg (92 %, assuming complete conversion)

Characterization in line with previous reported data.[35]

Metalation:

For a typical metalation, 50 mg PyrBpyCMP were dispersed in 4 ml acetonitrile, then 0.32 ml of a 0.015 M suspension of $[Cp^*RhCl_2]_2$ in acetonitrile were added and the suspension was stirred for 24 h at room temperature. The supernatant was removed by centrifugation and the solid washed with MeOH until the supernatant after centrifugation remains colourless. The solid was dried under reduced pressure first at room temperature, then at 80°C.[38]

1.3. UV-vis steady state and time-resolved spectroscopic measurements

All the spectroscopic measurements were performed using spectrophotometric grade solvents without any additional purification. The solvents used are acetonitrile (MeCN), propionitrile (ProCN), butyronitrile (BuCN), and tetrahydrofuran (THF). The triethanolamine (TEOA) was mixed with MeCN in the proportion MeCN:TEOA (5:1) that corresponds to the photocatalytic conditions applied in reference [35], or with THF, in the same proportion THF:TEOA (5:1). No other ratio was used in this work.

A Cary 100 UV-vis spectrometer (Varian) and a fluorometer Cary Eclipse (Agilent Technologies) were used for the steady state absorption and emission measurements, respectively. All the measurements were performed using 10*10 mm quartz optical cell. The time-resolved emission measurements were carried out by using the time-correlated single photon counting (TCSPC) set-up described in ref [39]. Briefly, the excitation pulses were generated by a femtosecond Ti:sapphire laser (Coherent Chameleon Ultra II, 80 MHz, 200 fs, 3.8 W) coupled with a pulse picker (4 MHz) and a harmonic generator (SHG/THG, APE). The fluorescence lifetime measurements were carried out with the FT200 PicoQuant spectrometer and the emission signal was collected with a polarizer set at the magic-angle and a Czerny-Turner type monochromator connected to a computer for observation wavelength selection. The photons were collected with a cooled microchannel plate photomultiplier tube R3809U (Hamamatsu) and recorded using a PicoHarp 300 TCSPC system (PicoQuant). The instrumental response function (IRF) was measured using Ludox colloidal solution and the full width at half maximum (FWHM) was found to be 50 ps. For these experiments, the emission was collected at 90 degrees using a 10*10 mm optical cell. The software used to plot and process the decays was FluoFit

v.4.6.6 (PicoQuant) and a home-made python script. The excitation wavelength used for each compound is given in the text.

UV-vis femtosecond transient absorption measurements were performed using an upgraded pump-probe experimental arrangement[40] derived from the original described in ref.[41] Briefly, the laser pump excitation was generated by using an OPA (Model Palitra, Quantronix) seeded by the fundamental laser pulses at 800 nm from the Ti:Sa amplifier (Libra Coherent, 1mJ, 1kHz, 100 fs). The synchronized probe beam is a white light supercontinuum covering the 320-800 nm spectral range and generated by focusing a few µJ of the fundamental laser pulses at 800 nm into a moving CaF_2 plate. Before the sample, the probe beam is split in a signal and reference beam, both passing through the sample and detected simultaneously by a liquid nitrogen-cooled CCD camera (Model Pylon, Princeton Instrument) placed in the image plane of a spectrograph. The pump-probe acquisition is controlled by a pair of synchronized optical chopper at 66 Hz and 33 Hz, placed on the probe and pump beam path, respectively. The relative direction of polarization of the pump and probe beam is set at the magic angle (54.7°). The measurements for the molecular complex and the ligand were performed using a flowing quartz cell with an internal optical path 1 mm. For the polymers in suspension, the measurements were carried out in 10 mm thick optical cell. With the flowing cell, the pump-probe cross-correlation FWHM deduced from the stimulated Raman contribution is ca. 130 fs.

2. Results-Discussion

2.1. Femtosecond UV-vis transient absorption measurements on PyrBpyCMP and Cp*Rh@PyrBpyCMP porous polymers

The steady state and time-resolved emission properties of **PyrBpyCMP** and **Cp*Rh@PyrBpyCMP** have been reported previously [35]. While these preliminary results clearly demonstrated the efficient energy transfer from the organic matrix to the RhCp* complex, that was interpreted as the activation of the catalytic metal centre, they provided few information concerning the nature of the excited states responsible of the processes. In order to clarify the nature of the excited states formed upon the photoexcitation of **PyrBpyCMP** and **Cp*Rh@PyrBpyCMP** we performed the first fs transient absorption measurements for this family of porous polymers. For the measurements, the polymers were suspended in MeCN:TEOA (5:1) solutions. We point-out here the difficulties of these transient absorption measurements because the polymers are insoluble in any common organic solvent and so, the suspension are highly scattering our supercontinuum probe and the pump beam. So, to carry out these measurements, we had to work by using a standard 1 cm quartz cell, in which the stability and the optical density of the suspension were compatible with the experimental constrains, but at the cost of a degraded time-resolution. We also took all the common precautions by checking the linearity of our signal with the pump intensity and the photostability of the sample. The viscous TEOA helps in stabilizing the suspension, but in counterpart, it generates a strong transient signal. Due to this measurement conditions, we limit our analysis to the pump-probe delays longer than 5 ps, for which we obtained reliable transient spectra (**Figure 1-a**). At 5 ps, the transient spectrum of **PyrBpyCMP** is dominated by a broad excited state absorption band from 485 nm to 750 nm, and a weak negative contribution at 475 nm suggesting a stimulated emission band between 450 and 500 nm. The transient absorption spectra exhibit a maximum of absorption at 700 nm and a second maxima at 550 nm. At 2 ns the signal is reduced to a residual absorption below 450 nm and a weak negative contribution from 500 to 700 nm. For **Cp*Rh@PyrBpyCMP**, the transient spectra in Figure 1.b are similar to **PyrBpyCMP**

and are essentially dominated by the excited state absorption from the organic part of the polymer. We cannot detect a clear signature that could be assigned to the activated metal centre. Instead, we notice a pronounce negative contribution, that seems to appear at very short time and is still observed in the ns time scale. We tentatively assigned this negative signal to the bleach of the charge transfer absorption band from the organic framework to the metal centre. We are also noticing that the kinetics of decay measured for the absorption band at 700 nm (Fig 1-c) is significantly slower in presence of the metal. So, these transient data reveal for both samples the formation of a large absorption that certainly corresponds to the signature of the excited organic framework. This signature is perturbed in presence of RhCp* but we cannot detect a clear absorption contribution specific of the activated catalytic centre. In order to elucidate the nature of the excited state of the CMP, we performed an exhaustive investigation of the **Pyr$_2$Bpy** and **Cp*Rh@Pyr$_2$Bpy** molecular compounds**.** These molecular compounds can be considered as building block of the CMP (**Scheme 1**). Our experimental approach is part of a general strategy aiming to develop molecular descriptors of the properties of the photoactive porous polymers that can orient the design of these photocatalysts. Similar approaches are also carried out at the theoretical level[35,42].

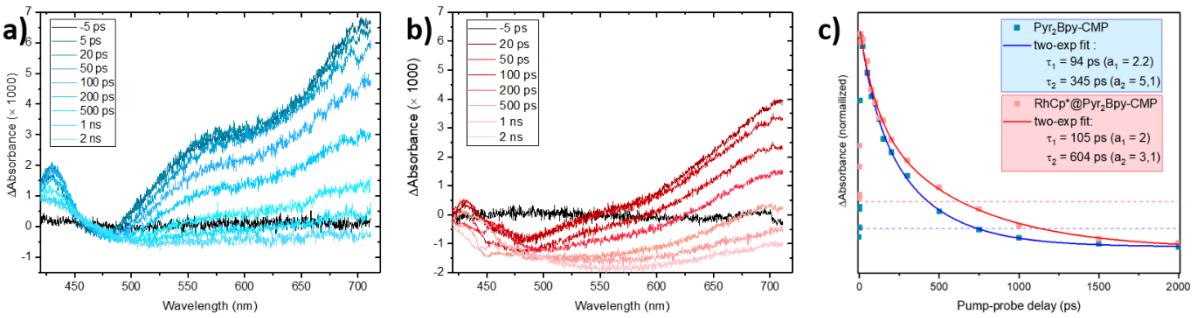

Fig. 1: Transient absorption spectra recorded with λ_{pump} = 400 nm for **a) PyrBpyCMP** and **b) Cp*Rh@PyrBpyCMP**, and **c)** the kinetic traces reconstructed at λ_{probe} = 700 nm and their corresponding fit. In Figure c), the decays have been normalized and the dotted lines correspond to the y=0 level of each curve.

2.2. 5,5'-di(pyren-1-yl)-2,2'-bipyridine molecular ligand (Pyr$_2$Bpy)

Part of the photophysical properties of **Pyr$_2$Bpy** have been first reported by E. Orti and co-workers[37] in the context of their study of [Ir(Ppy)$_2$(Pyr$_2$Bpy), with Ppy = phenylpyridine. As **Pyr$_2$Bpy** is poorly soluble in most of the common solvents[37], we limited our investigations to THF, a solvent for which the solubility is high enough to carry out femtosecond transient absorption measurements of the ligand. The absorption spectrum of **Pyr$_2$Bpy** exhibits a set of relatively narrow peak between 250 nm and 330 nm corresponding to $S_0 \rightarrow S_n$ electronic transition localized on the bipyridine and pyrene moiety and a broad featureless band with a maximum at 360 nm assigned to the HOMO-LUMO transition involving an electronic density delocalized over the whole ligand (**Figure 2**) [35,37]. The photoluminescence spectrum excited at 350 nm shows a strong emission band with a maximum at 442 nm. The excitation spectrum recorded at λ_{em} = 440 nm corresponds to the absorption spectrum (**Figure 2.a**).

In addition, we have determined the emission yield for λ_{exc} = 380 nm, to be ϕ_{em} = 0.78 (see SI). The transient emission spectra of **Pyr$_2$Bpy** have been characterized by TCSPC measurements (**Figure 2b**). We observe a unique emission band that is decreasing without spectral change and with a shape and maximum that correspond to the steady state emission spectrum. The decay trace at the maximum (440 nm) is well fitted using a mono-exponential decay function, with τ_{THF}= 1.4 ns. The spectra and the value that we obtained for **Pyr$_2$Bpy** in THF are in good agreement with the data reported for toluene (ϕ_{em} = 0.88, τ = 1.4 ns), dichloromethane (ϕ_{em} = 0.62, τ = 1.7 ns) and acetonitrile (ϕ_{em} = 0.42, τ = 2.4 ns).[37] This emission band is unambiguously assigned to the lowest singlet excited state (S_1) of **Pyr$_2$Bpy**. Based on the literature data, the nature of this excited state is not changed by the polarity of the solvent.

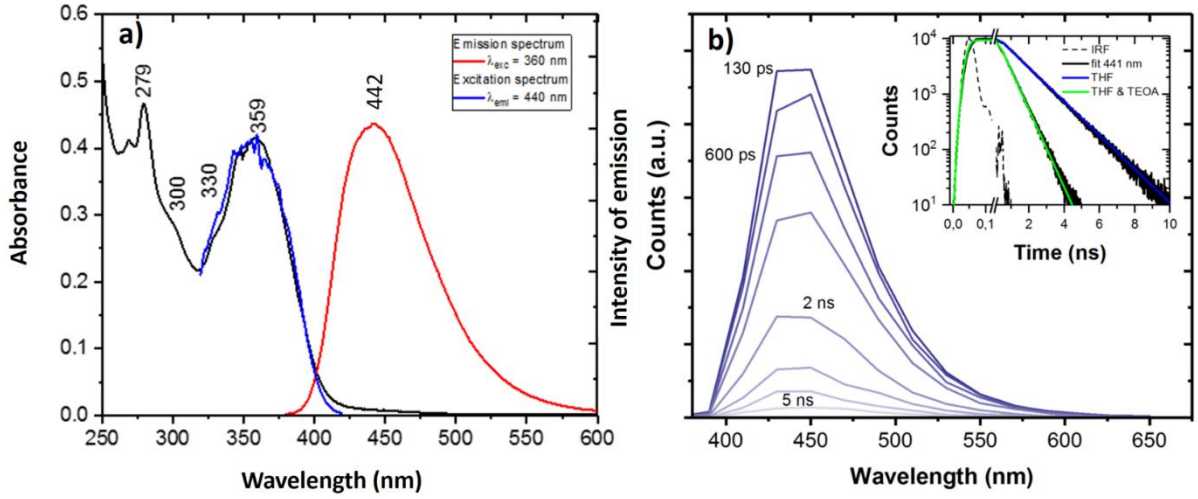

Fig. 2: a) Absorption (black), emission for λ_{exc} = 360 nm (red) and excitation spectrum for λ_{em} = 440 nm, of **Pyr$_2$Bpy** in THF; **b)** transient emission spectra of **Pyr$_2$Bpy** in THF, inset emission decay traces and the corresponding fits for **Pyr$_2$Bpy** in THF (blue line) and THF:TEOA, 5:1 volume ratio, (green line).

TCSPC measurements were also performed in THF:TEOA solution at the volume ratio 5:1 corresponding to the typical condition of the CO_2 photoreduction [32,39]. TEOA can be irreversibly oxidized (E_{NHE} = + 0.5-07 V) as sacrificial electron donor to regenerate the photosensitizer or, depending on the reaction conditions, it can act as a Brønsted base when associated with another sacrificial electron donor[46–48]. The emission lifetime measurement allows to determine directly if TEAO, at high concentration in the THF:TEOA mixture, can interact directly with the excited state of **Pyr$_2$Bpy** or if TEOA behaves essentially as a sacrificial electron donor reacting after a potential oxidation of **Pyr$_2$Bpy** during the CO_2 reduction cycle. The addition of TEAO accelerates significantly the emission decay in comparison to the case of neat THF (**Figure 2b**). The emission spectrum of **Pyr$_2$Bpy** is not modified (**Figure SI-2.1**) indicating that the nature of the emitting state of **Pyr$_2$Bpy** is also not affected by the presence of TEOA.

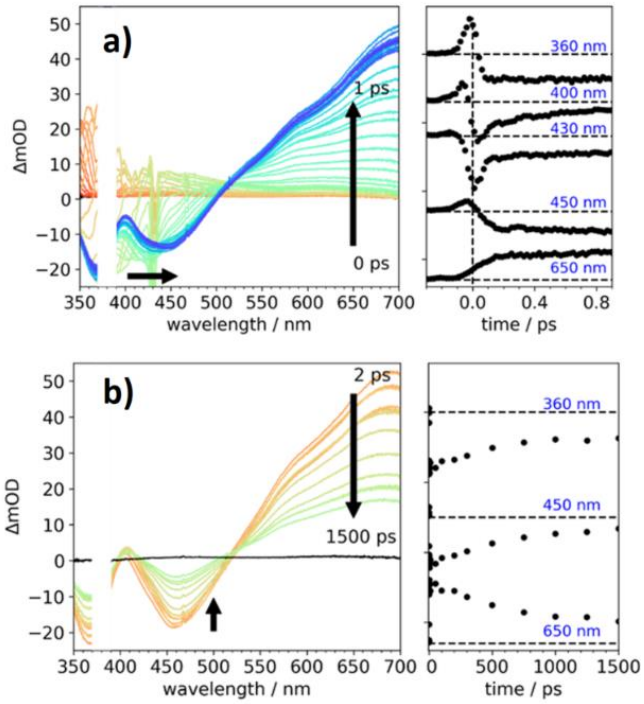

Fig. 3: Transient absorption spectra and selected kinetic traces recorded for **Pyr$_2$Bpy** in THF with λ_{pump} = 380 nm for pump-probe delays between **a)** 0 and 2 ps, and **b)** 2 ps and 1.5 ns

From the fit of the decay the lifetime of S_1 in the mixture is obtained to be $\tau_{THF:TEOA}$ = 0.7 ns. By comparing the lifetime in pure THF and THF:TEOA mixture, the decay time associated with the reaction of the excited **Pyr$_2$Bpy** with TEOA is τ_{TEOA} = 0.7 ns. With a concentration of TEAO of 1.25 mol·L^{-1} and assuming a pseudo-first order decay, the rate constant for the quenching of the S_1 state of **Pyr$_2$Bpy** by TEOA is k = 1.14×10^9 L·mol^{-1}·s^{-1}. From this value, it can be concluded that at molar concentration of TEOA, as it is usually the case for photocatalytic reactions condition using this amine as sacrificial electron donor, the excited states **Pyr$_2$Bpy,** and probably of other pyrene-aryl derivatives, with a lifetime as short as 200-300 ps can directly react with the amine**.**

In order to get a better insight of the S_1 state of **Pyr$_2$Bpy** and also on its reaction with TEOA**,** femtosecond transient absorption spectra (TAS) of **Pyr$_2$Bpy** were recorded in THF (**Figure 3**. The transient spectra recorded for pump-probe delays shorter than 150-200 fs are dominated by the contribution of the impulsive response of the solvent. After 200 fs the transient spectra show two negative bands in the spectral range below 500 nm. The first band is formed in less than 200 fs and it exhibits a maximum at 360 nm that corresponds to the $S_0 \rightarrow S_1$ absorption band (**Figure 2**). This contribution is due to the bleaching of the ground state of **Pyr$_2$Bpy**, i.e. the decrease of the absorption due to the depopulation of the ground state upon the photoexcitation. We notice in **Figure 3a**, and notably in the kinetic trace reconstructed for λ_{probe} = 360 nm, that the amplitude of the bleach signal is constant during the first picosecond, indicating that there is no ultrafast internal conversion involved in the photophysical process of **Pyr$_2$Bpy** in THF. The maximum of the second negative shifts continuously from ca. 400 nm to 450 nm during the two first picosecond. The final position with a maximum close to 450 nm is in good agreement with the emission band (**Figure 2**) and therefor, this

band is assigned to the excited-state stimulated emission of the S_1 state of **Pyr_2Bpy**. In the spectral range above 400 nm, the transient spectra exhibit a strong, broad and slightly structured absorption band with a maximum peaking above 700 nm that characterize the absorption of the S_1 state. In the kinetic traces between 150 fs and 1 ps, the formation of the excited state absorption band occurs concomitantly with the spectral shift of the stimulated emission illustrated for λ_{probe} = 400 nm and λ_{probe} = 450 nm. On the longer timescale, from 1 ps to 1500 ps (**Figure 3b**) the shape of the transient spectra does not change, only the amplitude of the signal decreases, resulting in an isobestic point at 530 nm. The decay of the signal is not completed after 1.5 ns, in good agreement with the lifetime deduced from the TCSPC data. The transient spectra evolution reveals the decay of the excited state without any spectral signature of the conversion of the S_1 state into a new transient species. Thus, the internal conversion from the S_1 to the S_0 state by emission represents the main relaxation channel of **Pyr_2Bpy**.

The nature of the lowest excited state of aryl-pyrene derivatives results in the competition between the stabilization of a planar geometry by Mesomeric Intramolecular Charge Transfer (**MICT**) and the stabilisation in a Twisted Intramolecular Charge Transfer (**TICT**) state by a perpendicular orientation of the pyrene and pyridyl moiety.[46,47] By combining the photoluminescence, TCSPC and transient absorption results, we deduced that following the excitation of **Pyr_2Bpy** at 380 nm a MICT state is formed within approx. 1-2 ps by a charge delocalisation from the pyrene to the bipyridine moiety. After this initial step, the S_1 state of **Pyr_2Bpy** decays mainly by emission (ϕ_{em} = 78 %, in THF) and with a relatively short lifetime of 1.4 ns, in good agreement with the strong emission oscillator strength expected from a **MICT** state[47]. This description is in good agreement with results from steady state emission measurements of **Pyr_2Bpy** in different solvent reported by Ortí and co-workers[37], and with the result of quantum calculations showing the planarization of the molecule in the S_1 excited state due to the extension of the π-conjugation over the **Pyr_2BPY** molecule [35].

In order to explain the process of quenching of the emission of the S_1 state of **Pyr_2Bpy** by TEAO, we also performed the transient absorption study of **Pyr_2Bpy** in the THF:TEOA (5:1) mixtures. As TEOA is an electron donor, we can notably expect the observation of the anion of **Pyr_2Bpy** in case of electron transfer. In fact, the ultrafast photodynamic recorded in THF:TEOA (**Figure SI-3.1**) is very close to that observed in pure THF (**Figure 3**), and only the spectral signature of the S_1 state of **Pyr_2Bpy** is identified in the transient spectra. These data are showing that the quenching of the S_1 of by **TEOA** does not lead to the stabilization of a reduced separated ion pair (SIP). Furthermore, we can rule out the hypothesis that the TEOA favor the direct internal conversion $S_1 \rightarrow S_0$ because we observed in THF and THF:TEOA the same emission spectra and stimulated emission band resulting from the π-delocalization of the LUMO (MICT state). Thus, the quenching of the S_1 state of **Pyr_2Bpy** by TEOA is more likely a reductive quenching followed by the ultrafast recombination of the geminate pair [$TEOA^+$, Pyr_2Bpy^-]. The low polarity and the viscosity of the THF:TEOA mixture might facilitate the intrapair geminate recombination (**Scheme 2**). Similar results have been reported for the photoreduction of the $n\pi^*$ S_1 state of the 4,4'-bipyridine for which intrapair recombination was found to be the main deactivation path (ϕ_{deact} = 95 %) even in highly polar dielectric solvent (MeCN, MeCN-H_2O mixture) [48,49]. In many photocatalytic applications, TEOA is introduced as a sacrificial electron donor. Our result show that at high concentration it can interact directly with some excited state of the photosensitized ligand, and thus contributes to the reduction of the overall photocatalytic yield by quenching the excited state because the deactivated excited state will not contribute anymore to the activation of the catalytic site. This point can be particularly important in the context of our **PyrBpy** porous polymer for which

the Pyrene-Bipyridyl moieties constitute the backbone of the porous artificial antenna in which TEOA are adsorbed. Under these conditions, the excited state interaction and quenching can strongly compete with the photoactivation of the catalytic site.

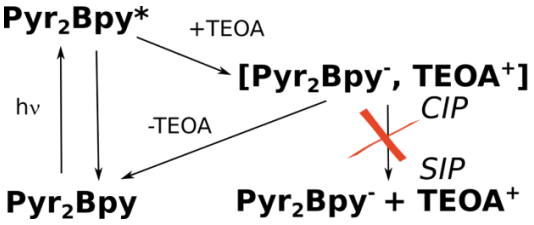

Scheme 2: Photoreaction of **Pyr_2Bpy** in THF:TEOA. CPI = Contact Ion Pair, SIP = Separated Ion Pair.

2.3. [(5,5'-di(pyren-1-yl)-2,2'-bipyridine)(pentamethyl-cyclopentadienyl)rhodium] dichloride complex ([Pyr_2Bpy]Cp*$RhCl_2$)

In this section, we are reporting on the ultrafast photodynamics following the photoexcitation of the molecular complex **[Pyr_2Bpy]Cp*$RhCl_2$** in acetonitrile (MeCN, ε = 37.5), the solvent typically used for the photocatalytic CO_2 reduction, propionitrile (ProCN, ε = 27.7) and butyronitrile (BuCN ε = 20.7). The UV-vis absorption spectra recorded for **[Pyr_2Bpy]Cp*$RhCl_2$** in MeCN, ProCN, BuCN are depicted in **Figure 4**. In the three solvents, the absorption spectrum of the complex exhibits a first absorption band with a maximum peaking at 420 nm and a set of narrow peak typical of the pyrene unit around 330 nm. The lowest optical transition at 420 nm is 70 nm red-shifted in comparison with the free **Pyr_2Bpy** ligand in THF. The absorption spectrum of **[Pyr_2Bpy]Cp*$RhCl_2$** in MeCN is similar to that one of protonated **[Pyr_2BpyH]$^+$** [37] . Considering that the proton H^+ is equivalent to a reduced form of the Rhodium cation, the similitude in the absorption is suggesting a charge transfer from the Bpy to the metal center.[37] This is also demonstrated by DFT calculation of the HOMO/LUMO of **[Pyr_2Bpy]Cp*$RhCl_2$** showing that the lowest transition correspond to a charge transfer from the pyrene moieties towards the bipyridine-rhodium moiety.[35] We can observe in ProCN and BuCN a slight decrease of the relative intensity of the lowest absorption band and an increase of the absorption at 350-375 nm for BuCN. The polarity of solvent is known to assists the charge separation, therefore this effect support the assignment of the lowest optical transition to a charge transfer between the photoactive pyrene chromophore and the bipyridine-rhodium centre forming a **TICT** state.[46,47] Contrary to the S_1 state of the **Pyr_2Bpy** molecular ligand, the lowest excited state of **[Pyr_2Bpy]Cp*$RhCl_2$** is weakly fluorescent (ϕ < 1 %) with an emission maximum at 620 nm when excited at 420 nm (**Fig. SI-1-2**) and it decays within less than 200 ps (**Fig. SI-2-2**).

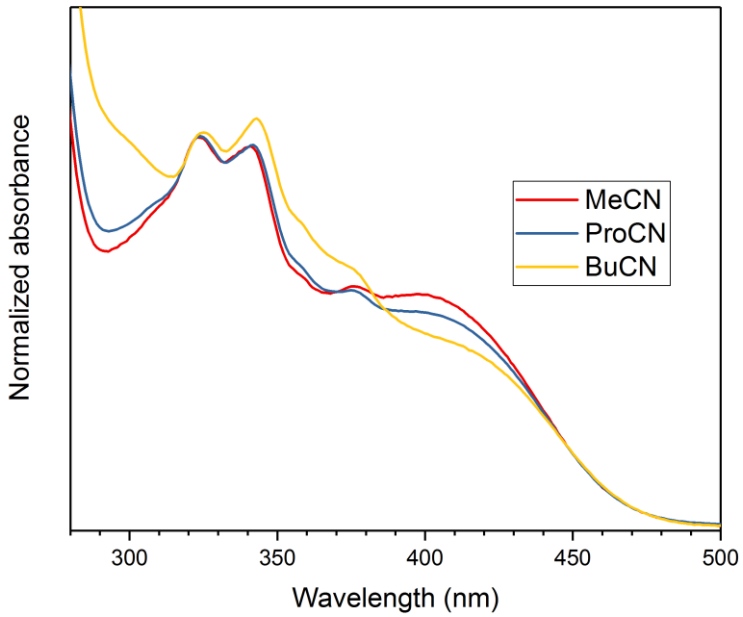

Fig 4: Absorption spectrum of **[py$_2$(Bpy)]Cp*RhCl$_2$** in Acetonitrile (MeCN, red), Propionitrile (ProCN; blue) and Butyronitrile (BuCN, yellow)

We focused our study on the characterization of the excited state by carrying out femtosecond transient absorption measurement using a pump in resonance with the lowest $S_0 \rightarrow S_n$ optical transition (λ_{pump} = 400 nm). The transient absorption data of **[Pyr$_2$Bpy]Cp*RhCl$_2$** in MeCN are reported in **Figure 5** for selected pump-probe delays between -200 fs and 1.2 ps and in **Figure 6** for delays up to 1.5 ns. The transient spectra show the ultrafast continuous interconversion between a first excited state absorption band exhibiting a maximum at 620 nm (**ESA1**) and a second absorption band peaking at 520 nm (**ESA2**). **ESA1** is formed in less than 150 fs and it decays within 300-500 fs. In addition, the transient spectra exhibit a ground state bleach (**GSB**) contribution between 360 – 420 nm. In **Figure 5c** we selected three spectra representative of the ultrafast sub-ps photodynamic of the system. Qualitatively, the first step is identified at Δt = 0.14 ps, by the absorption **ESA1**, the negative **GSB** contribution, and in addition a second minimum at 500 nm that corresponds to the stimulated emission contribution (**SE**) from the generated excited state. **SE** is continuously red-shifted and decreasing (step 2, from ca 0.1 ps to 0.3 ps). Between 0.3 and 1 ps (step 3) we observe the conversion of **ESA1** into **ESA2** with an isobestic point at 580 nm. The amplitude of **GSB** (420 nm) is constant during this phase, showing the absence of internal conversion to the ground state. Based on these transient spectra, the ultrafast sub-ps photodynamic of **[Pyr$_2$Bpy]Cp*RhCl$_2$** corresponds to the population of the S_n excited state by absorption of the photon at 400 nm, followed by an ultrafast evolution of the Franck-Condon geometry in response to the instantaneous change of the electronic density, and then,

the subsequent internal conversion to the S_1 state. This behaviour is typical of the ultrafast conversion between the close lying S_2 and S_1 excited state of pyrene and pyrene derivatives[50–53].

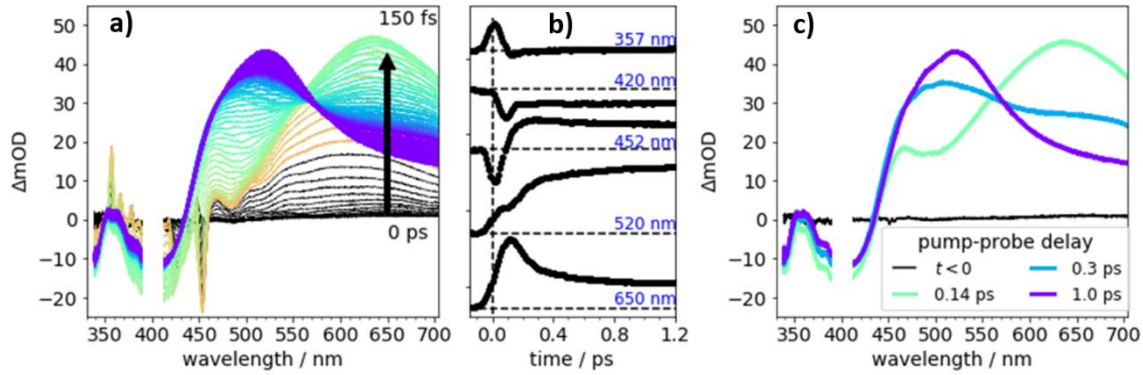

Fig. 5: Transient absorption spectra (a, c) and selected reconstructed kinetic traces (b) for **[pyr$_2$(Bpy)]Cp*RhCl$_2$** measured in MeCN with λ_{pump} = 400 nm. In (a) the pump-probe delay steps are 10 fs. The spectra have been corrected from the GVD of the supercontinuum probe using a polynomial model function.

The transient spectra were measured for the complex in MeCN, ProCN and BuCN, and in the solution MeCN:TEOA, ProCN:TEOA and BuCN:TEOA, for pump-probe delays up to 1.5 ns. The results are depicted in **Figure 6**, and in SI-section 3.b. In MeCN, after the ultrafast $S_2 \rightarrow S_1$ conversion (**Fig 6a**), the transient spectra in **Fig 6b** are dominated by a broad absorption band peaking at 530 nm. After 500 ps, the broad band is replaced by two weak absorption maxima at 520 nm and 600 nm, respectively, and that are still observed after 1.5 ns. The decay of the absorption band of S_1 (530 nm) is clearly associated with the diminishing of the GSB contribution. The same spectral evolution is observed in propionitrile (see SI **Fig SI-3-2**). In butyronitrile, the ultrafast S_2-S_1 conversion is observed in 5 ps (**Fig 6c**) and we are noticing that the absorption band at 650 nm is lasting to the nanosecond time scale. The transient absorption after 1.5 ns is significantly more important in BuCN than in MeCN, notably due to the more pronounce component at 650 nm. The dynamics of conversion $S_2 \rightarrow S_1$ is also significantly slower in BuCN, as it is clearly seen in the traces of **Figure 7**. From the fit of the decay, the growing time of the band at 530 nm is 360 fs in MeCN and 0.9 ps in BuCN. In MeCN, the band at 530 decays with two times constants τ_1 = 14 ps and τ_2 = 37 ps (see SI), while in BuCN, the process is slower with τ_1 = 33 ps and τ_2 = 225 ps (see SI). We also performed transient measurements in the presence of TEAO. In MeCN:TEOA, the process is not modified compared to the process in pure MeCN, excepted a slight increase of the decay time at 530 nm, but without consequence of the final spectra at 1.5 ns. For BuCN, we observe an increase of intensity and lifetime of the absorption band at 530 nm (**Figure 6** and **7**). The spectrum at 1.5 ns exhibits more absorption contribution at 530 nm, and more bleach contribution in BuCN:TEOA than in BuCN. Interestingly, while in ProCN the transient data are similar to that measured in MeCN, while in ProCN:TEAO (see SI section 3-2) we can notice a transient absorption at 1.5 ns that is very close to that observed in BuCN:TEAO (see SI section 3-2).

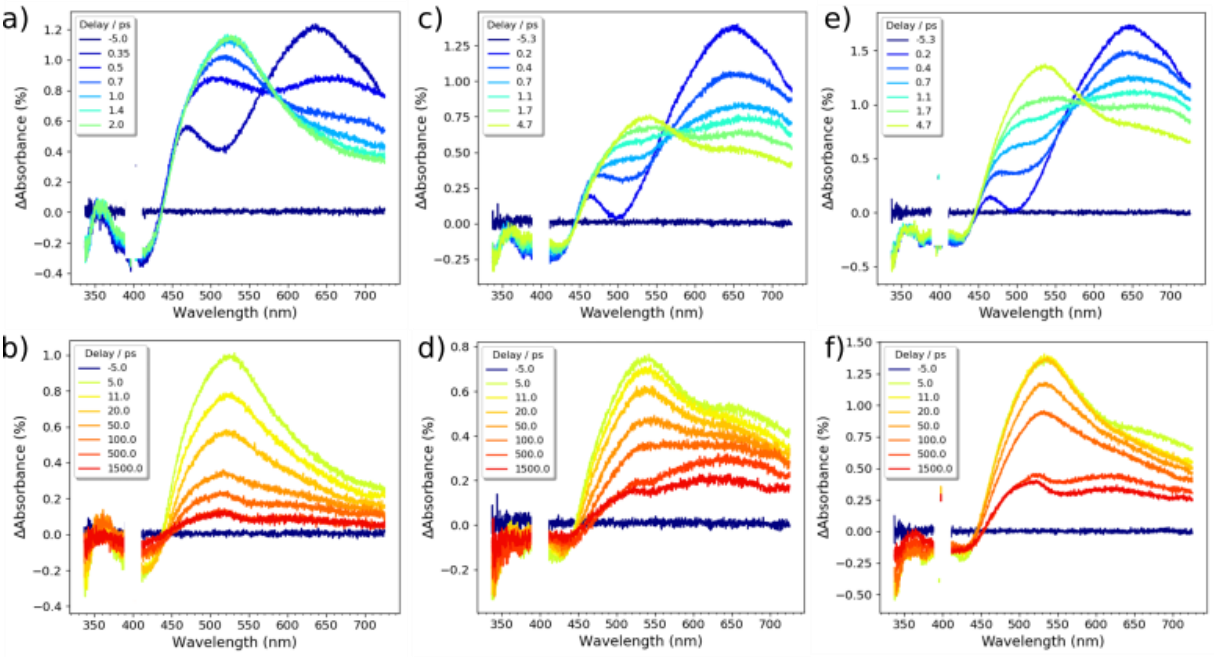

Fig. 6: Transient absorption spectra of **[py$_2$(Bpy)]Cp*RhCl$_2$** (λ_{pump} = 400 nm) In (a,b) MeCN, (c,d) BuCN, and (e,f) BuCN:TEOA

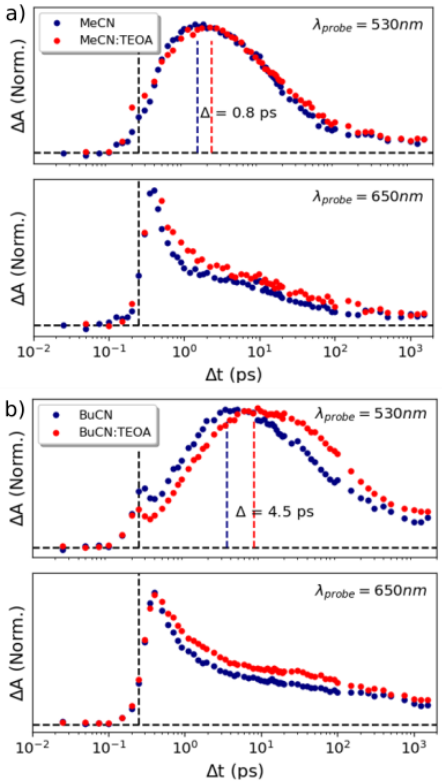

Fig. 7 Decay trace of **[Pyr$_2$Bpy]Cp*RhCl$_2$** (λ_{pump} = 400 nm) In (a) MeCN and MeCN:TEOA, and (b) BuCN and BuCN:TEOA.

The sub-ns photodynamics measured for the molecular complex **[Pyr$_2$Bpy]Cp*RhCl$_2$** can be described based on the photophysic of the excited-states of the aryl-substituted pyrene molecular derivatives.[46,47,50-53] For the **[Pyr$_2$Bpy]Cp*RhCl$_2$** compounds. the transient spectrum detected immediately after the pump excitation (Δt = 100-200 fs in **Figure 5** and **Figure 6**) is similar to that one of the molecular ligands (**Fig 4**) showing the formation of a MICT state delocalized over the Py$_2$Bpy ligand part of the compounds. It is then converted within a few hundreds of femtoseconds into a combination of the MICT and TICT state of the ligand. In MeCN, the TICT is favoured by the polarity of the solvent while, as the polarity of the solvent is reduced in BuCN, the mixing between the MICT and TICT is more pronounced and we observed the presence of the two maxima (530 nm and 650 nm) suggesting that the two configurations of the excited ligand are in equilibrium. This excited state decays time in the 10 ps-100 ps range corresponds to the formation of the ligand to metal (LMCT) charge transfer state from the excited ligand to the Rh^{3+} centre. This assignment is supported by the DFT calculation[35]. Our time-resolved data revealed the presence of two absorption band at 520 nm and 600 nm after 1.5 ns suggesting the co-existence of two different conformers that we tentatively propose as the asymmetric and the symmetric charge transfer, involving respectively one or two pyrene moieties (**Scheme 3**). The existence of two conformer and two reaction channels is supported by the difference in the kinetic at 530 nm and 650 nm. However, additional kinetics analysis and time-resolved measurements (structural or vibrational, for examples) are necessary to precise the nature and the yields of formation of these different LMCT species.

From the data in **Figure 5** and **SI-3-2**, we can characterize the effects of **TEOA** on the excited states of the complex. First, we didn't observe the formation of any new species, nor a reduction of the lifetime of the excited state in presence of TEOA, meaning that there is no electron transfer or quenching mechanism involved in the process. This point is in good agreement with the rate constant of electron transfer calculated for the ligand in THF (Section 2.1). In MeCN, TEOA has no effect on the transient dynamics and species observed bellow 1.5 ns. This is clearly different for ProCN, and BuCN for which we observed a clear increase of lifetime of the excited state localized on the ligand and consequently a different proportion of different LMCT conformers stabilized at 1.5 ns. It is notably worth noting that in BuCN:TEOA and ProCN:TEOA, the bleach signal is quasi-constant in the sub-ns time scale and a more efficient formation of the LMCT state is observed. The stabilization of the LMCT state result therefore of a complex synergy between the polarity of the solvent governing the MICT /TICT character of the excited state, and the viscosity of the TEOA solution constraining the twisting motion around the pyrene and bipyridine C-C bond. We concluded that, at high concentration, the TEOA molecules are not simple spectators of the photodynamic of the **Pyr$_2$Bpy** derivatives, as it is often assumed but they can also deactivate the excited states of the ligand (MLCT sate) or affect the degree of π-conjugation and charge transfer to the metal, notably by acting on the twisting dynamics around the interring C-C bond, that is a particularly critic parameter affecting the nature and the yield of formation the catalytically active LMCT species. We anticipate that this effect can be extending to other family of organo-metallic catalysts and should be more carefully considered in the design of the photocatalytic process.

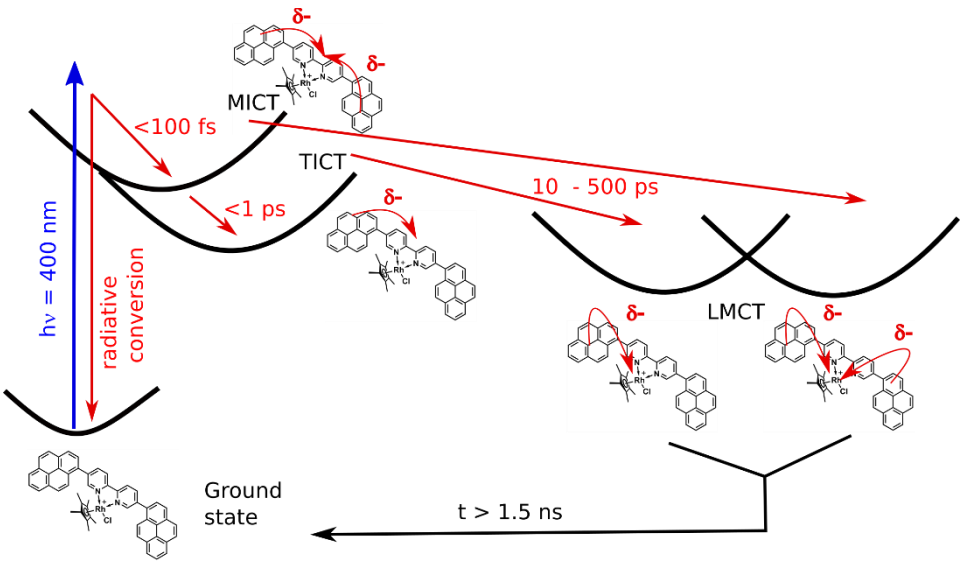

Scheme 3: Excited state relaxation pathways of **[pyr$_2$(Bpy)]Cp*RhCl$_2$** following a photoexcitation at 400 nm, MICT, TICT and LMCT, means mesomeric, twisted intramolecular and ligand-to-metal charge transfer, respectively. The time in the figure are approximated values from the decays in Figure 7.

2.4. From the molecular model compounds to the Pyrene-bipyridine porous polymers (PyBpy-CMP)

In the last part of this discussion, we will connect the photophysical and photochemical properties of the CMP with that of the molecular compounds. The steady state and time-resolved emission properties of **PyrBpyCMP** and **Cp*Rh@PyrBpyCMP** have been reported by us in a previous study [35]. Briefly, both materials exhibit a dual emission band. A first emission around 490 nm and corresponding to an excitation band centred at 375 nm and second emission extending from 500 nm to 750 nm and associated with an excitation spectrum with a band edge at 525 nm. In our previous paper, we described the first emission as localized of the PyrBpy chromophe (LE) and the second red-shifted contribution has been assigned to an internal charge transfer (ICT) emission involving a more pronounce charge transfer from the pyrene to the surrounding bipyridine moieties.[35] From the emission properties of the molecular ligand **Pyr$_2$Bpy** and for the molecular complex reported in this work, we can clearly correlate the LE emission bands of **PyrBpyCMP** to the emission of pyrene-bipyridine-pyrene conformation similar to that of the MICT state of the **Pyr$_2$Bpy** molecular ligand (470 nm) and the ICT emission to that of a molecular conformation similar to that of the TICT state (650 nm) from the ligand part of the molecular complex, respectively. We notice however that the lifetime of the emission for **PyrBpyCMP** are significantly shorter that for the molecular compounds. Notably for the LE emission of the polymer, we found in MeCN and MeCN:TEOA[35] a lifetime of 110 ps, in comparison to lifetimes above 700 ps for the molecular **Pyr$_2$Bpy** ligand (2.4 ns in MeCN,[37] 1.4 ns in THF and 0.7 ns in THF:TEOA). This shows that the spatial arrangement of the polymer favours the internal conversion processes in comparison with the free molecular ligand. This can be understood by the fact that the 3D arrangement in the polymers induces some torsion around the pyrene – bipyridine bond.

In addition, we can notice (**Figure 1**), that the transient absorption spectra of the **CMP** exhibit a maximum of absorption at 700 nm and a second maxima at 550 nm. similar to the transient absorption band measured for the molecular models. We therefore tentatively assigned these the transient absorption bands of the CMP to the MICT and TICT contribution, in agreement with the conclusion

deduced from the time-resolved emission data that two forms of exciting states are coexisting in the porous polymer.

The light-harvesting and energy diffusion process governing the light-to-chemical energy conversion applications of porous organic materials is subject to highly intensive researches showing the complex interplay between the photophysical properties of the framework and its topology[11,12,54–58]. Among the different mechanisms, the Förster resonance energy transfer (FRET) mechanism is assumed to contribute as a main part of the process in most of the case. The Förster model establishes a relationship between the energy transfer rate k_{ET} and the absorption and emission spectra of the molecules, given by:

$$k_{ET} = \frac{1}{\tau_{fl}} \frac{{R_0}^6}{R^6}$$

$${R_0}^6 = \frac{9000 \cdot \ln(10) \cdot \phi_{fl} \cdot \kappa^2}{128 \cdot \pi^5 \cdot N_A \cdot n^4} \int_0^\infty \varepsilon(\nu) \cdot f(\nu) \frac{d\nu}{\nu^4}$$

with

- R_0 is the Förster critic radius, at which the lifetime of the donor is reduced by 50 %
- κ^2 is an orientational parameter, n is the refractive index of the medium
- ϕ_{fl}, the fluorescence yield of the donor
- $\varepsilon(\nu)$ the absorption spectrum of the acceptor (in molar absorbance), $f(\nu)$, the emission spectrum whose integral has been normalized to 1, and N_A the Avogadro number.

Here, we assume that the CMP can be viewed as a sum of independent molecular units and, by using the photophysical parameters determined for the molecular model clusters, we applied the Förster model to estimate the rate of the energy transfer depending on the distance between the different **pyrene** chromophores and the **Cp*Rh(Bpy)** centers in **Cp*Rh@PyrBpyCMP** (see SI, **Scheme 4**). This basic analysis suggests that at the Rh:Bpy loading of 1:12 used in this work, the energy transfer can occur faster than 50 ps. This value is in good agreement with the quenching time determined by TCSPC measurements, and with the decay determined from the TAS measurements. It seems therefore reasonable to describe the photoactivation of the Rh metal center as an ultrafast transfer of excitation from a localized excited state of the Pyr_2Bpy unit of the framework to a localized excited state of the **[Pyr_2Bpy]Cp*Rh** metal centre forming of the active charge separated state between the pyrene and the **Cp*Rh(Bpy)** moiety as theoretically predicted[35].

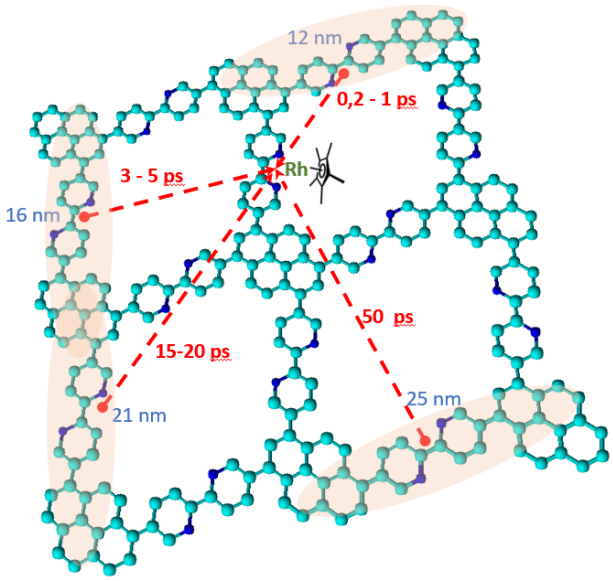

Scheme 4: Typical distances and times associated to the FRET energy between the **pyrene** units and the **Cp*Rh(Bpy)** centre in **Cp*Rh@PyrBpyCMP**. Assuming the ratio Rh:bipyridine of 1:12 in **Cp*Rh@PyrBpyCMP** as used in ref. [35],

Conclusions

We have investigated the excited states of molecular **Pyr_2Bpy** and **$[Pyr_2Bpy]Cp^*RhCl_2$** as molecular model of the corresponding photoactive conjugated microporous polymers **PyrBpyCMP** and **Cp*Rh@PyrBpyCMP**. For both **Pyr_2Bpy** and **$[py_2(Bpy)]Cp^*RhCl_2$**, the first photogenerated excited state is a mesomeric intramolecular charge transfer (MICT) involving a large delocalization of the electron over the whole **Pyr_2Bpy** unit. For the molecular ligand in THF, this MICT state is stabilized by the planarization of the molecule in the excited state, while for the molecular complex **$[py_2(Bpy)]Cp^*RhCl_2$** the MICT is rapidly converted (< 1 ps) in a twisted intramolecular charge transfer (TICT) involving a charge separation between the pyrene and bipyridine moieties. The TICT is then converted within 10-100 ps into a LMCT species, corresponding to the activated form of the metal catalyst, with a ns lifetime. From the study in MeCN, ProCN and BuCN and in presence of TEOA, it appears that both the polarity and the viscosity of the reaction medium govern the formation of the LMCT state, suggesting that the degree of charge delocalization and probably also the torsional dynamics around the pyrene-bipyridine bond are critical parameters in the photoactivation process. We performed the first femtosecond transient absorption measurements on the family of **PyrBpy** porous polymers from which we identified the formation of **Pyr_2Bpy**-like MICT and TICT excited states upon the photoexcitation of the porous organic framework. We estimated from the time-resolved measurement and the FRET model, that these excited states can transfer the excitation to the catalytic metal center in less than 50 ps. Our results confirm the role of the **Pyr_2Bpy** framework as light-harvesting macroligand for the Rh active site. More important, our results clearly demonstrate the complex role of the TEOA molecules that cannot be considered in the photocatalytic process only as passive sacrificial electron donors. Indeed, TEOA can also quench directly the excited state leading to reduce efficiency, and can also modulate the textural constraints of the flexible porous framework with consequences on the nature, i.e.TICT and/or MICT, and the lifetime of the excited states.

Furthermore, we anticipate that this time-resolved study will provide several clues to improve the photocatalytic efficiency of the molecular organic antenna like **PyrBpy** units within a porous polymer network by (i) the control of the flexibility and topology of the framework that clearly control the ratio

and lifetime of the MICT and TICT states, by (ii) the optimization of the distribution of the metal catalyst based on the energy transfer efficiency, and by (iii) taking into account the interaction of the sacrificial electron donor present in high concentration in the porous polymer suspension. All these parameters are accessible by systematic time-resolved investigation of photoactive porous polymers, and in line with theoretical modeling, can drive the design of more efficient photocatalyst for the light-to-chemical energy conversion.

Acknowledgement:

V.d.W acknowledges financial support from the Chevreul institute (FR 2638), the Ministère de l'Enseignement Supérieur et de la Recherche, Région Hauts-de-France and FEDER and technical assistance by the engineers of the Pole SAM and MICE of LASIRE. Q.P acknowledges PhD funding from Région Hauts-de-France and University of Lille. A.G. and F.M.W. gratefully acknowledges financial support from CNRS through Momentum 2018 excellence grant.

References

(1) Dhakshinamoorthy, A.; Li, Z.; Garcia, H. Catalysis and Photocatalysis by Metal Organic Frameworks. *Chem. Soc. Rev.* **2018**, *47* (22), 8134–8172. https://doi.org/10.1039/C8CS00256H.

(2) Wisser, F. M.; Mohr, Y.; Quadrelli, E. A.; Canivet, J. Porous Macroligands: Materials for Heterogeneous Molecular Catalysis. *ChemCatChem* **2020**, *12* (5), 1270–1275. https://doi.org/10.1002/cctc.201902064.

(3) Stanley, P. M.; Haimerl, J.; Shustova, N. B.; Fischer, R. A.; Warnan, J. Merging Molecular Catalysts and Metal-Organic Frameworks for Photocatalytic Fuel Production. *Nat. Chem.* **2022**, *14* (12), 1342–1356. https://doi.org/10.1038/s41557-022-01093-x.

(4) Kramar, B. V.; Flanders, N. C.; Helweh, W.; Dichtel, W. R.; Hupp, J. T.; Chen, L. X. Light Harvesting Antenna Properties of Framework Solids. *Acc. Mater. Res.* **2022**, *3* (11), 1149–1159. https://doi.org/10.1021/accountsmr.2c00137.

(5) So, M. C.; Wiederrecht, G. P.; Mondloch, J. E.; Hupp, J. T.; Farha, O. K. Metal-Organic Framework Materials for Light-Harvesting and Energy Transfer. *Chem. Commun.* **2015**, *51* (17), 3501–3510. https://doi.org/10.1039/c4cc09596k.

(6) Yu, J.; Li, X.; Deria, P. Light-Harvesting in Porous Crystalline Compositions: Where We Stand toward Robust Metal-Organic Frameworks. *ACS Sustain. Chem. Eng.* **2019**, *7* (2), 1841–1854. https://doi.org/10.1021/acssuschemeng.8b05673.

(7) Goswami, S.; Yu, J.; Patwardhan, S.; Deria, P.; Hupp, J. T. Light-Harvesting “Antenna” Behavior in NU-1000. *ACS Energy Lett.* **2021**, *6* (3), 848–853. https://doi.org/10.1021/acsenergylett.0c02514.

(8) Nasalevich, M. A.; Van Der Veen, M.; Kapteijn, F.; Gascon, J. Metal-Organic Frameworks as Heterogeneous Photocatalysts: Advantages and Challenges. *CrystEngComm* **2014**, *16* (23), 4919–4926. https://doi.org/10.1039/c4ce00032c.

(9) Gutiérrez, M.; López-González, M.; Sánchez, F.; Douhal, A. Efficient Light Harvesting within a C153@Zr-Based MOF Embedded in a Polymeric Film: Spectral and Dynamical Characterization. *Phys. Chem. Chem. Phys.* **2017**, *19* (27), 17544–17552. https://doi.org/10.1039/c7cp02094e.

(10) Liu, L.; Lu, X.-Y.; Zhang, M.-L.; Ren, Y.-X.; Wang, J.-J.; Yang, X.-G. 2D MOF Nanosheets as an Artificial Light-Harvesting System with Enhanced Photoelectric Switching Performance. *Inorg. Chem. Front.* **2022**. https://doi.org/10.1039/d2qi00404f.

(11) Zhang, Q.; Zhang, C.; Cao, L.; Wang, Z.; An, B.; Lin, Z.; Huang, R.; Zhang, Z.; Wang, C.; Lin, W. Förster Energy Transport in Metal-Organic Frameworks Is beyond Step-by-Step Hopping. *J. Am. Chem. Soc.* **2016**, *138* (16), 5308–5315. https://doi.org/10.1021/jacs.6b01345.

(12) Rajasree, S. S.; Yu, J.; Pratik, S. M.; Li, X.; Wang, R.; Kumbhar, A. S.; Goswami, S.; Cramer, C. J.; Deria, P. Superradiance and Directional Exciton Migration in Metal-Organic Frameworks. *J. Am. Chem. Soc.* **2022**, *144* (3), 1396–1406. https://doi.org/10.1021/jacs.1c11979.

(13) Yu, J.; Anderson, R.; Li, X.; Xu, W.; Goswami, S.; Rajasree, S. S.; Maindan, K.; Gómez-Gualdrón, D. A.; Deria, P. Improving Energy Transfer within Metal-Organic Frameworks by Aligning Linker Transition Dipoles along the Framework Axis. *J. Am. Chem. Soc.* **2020**, *142* (25), 11192–11202. https://doi.org/10.1021/jacs.0c03949.

(14) Gutiérrez, M.; Sánchez, F.; Douhal, A. Competitive Excimer Formation and Energy Transfer in Zr-Based Heterolinker Metal–Organic Frameworks. *Chem. - Eur. J.* **2016**, *22* (37), 13072–13082. https://doi.org/10.1002/chem.201600669.

(15) Gutierrez, M.; Cohen, B.; Sánchez, F.; Douhal, A. Photochemistry of Zr-Based MOFs: Ligand-to-Cluster Charge Transfer, Energy Transfer and Excimer Formation, What Else Is There? *Phys. Chem. Chem. Phys.* **2016**, *18* (40), 27761–27774. https://doi.org/10.1039/c6cp03791g.

(16) Yu, J.; Park, J.; Van Wyk, A.; Rumbles, G.; Deria, P. Excited-State Electronic Properties in Zr-Based Metal-Organic Frameworks as a Function of a Topological Network. *J. Am. Chem. Soc.* **2018**, *140* (33), 10488–10496. https://doi.org/10.1021/jacs.8b04980.

(17) Shaikh, S. M.; Chakraborty, A.; Alatis, J.; Cai, M.; Danilov, E.; Morris, A. J. Light Harvesting and Energy Transfer in a Porphyrin-Based Metal Organic Framework. *Faraday Discuss.* **2019**, *216*, 174–190. https://doi.org/10.1039/c8fd00194d.
(18) Santaclara, J. G.; Nasalevich, M. A.; Castellanos, S.; Evers, W. H.; Spoor, F. C. M.; Rock, K.; Siebbeles, L. D. A.; Kapteijn, F.; Grozema, F.; Houtepen, A.; Gascon, J.; Hunger, J.; Van Der Veen, M. A. Organic Linker Defines the Excited-State Decay of Photocatalytic MIL-125(Ti)-Type Materials. *ChemSusChem* **2016**, *9* (4), 388–395. https://doi.org/10.1002/cssc.201501353.
(19) Van Der Veen, M. A.; Mazur, K.; Nasalevich, M.; Hurkmans, M.; Gascon, J.; Kapteijn, F.; Houtepen, A.; Grozema, F.; Bonn, M.; Hunger, J. Femtosecond Pump - Probe Spectroscopy Reveals the Photo-Excited State and Charge Transfer of a Photocatalytic Metal-Organic Framework; 2014. https://doi.org/10.1364/up.2014.08.tue.p2.21.
(20) Nasalevich, M. A.; Hendon, C. H.; Santaclara, J. G.; Svane, K.; Van Der Linden, B.; Veber, S. L.; Fedin, M. V.; Houtepen, A. J.; Van Der Veen, M. A.; Kapteijn, F.; Walsh, A.; Gascon, J. Electronic Origins of Photocatalytic Activity in D0 Metal Organic Frameworks. *Sci. Rep.* **2016**, *6*. https://doi.org/10.1038/srep23676.
(21) Chambers, M. B.; Wang, X.; Ellezam, L.; Ersen, O.; Fontecave, M.; Sanchez, C.; Rozes, L.; Mellot-Draznieks, C. Maximizing the Photocatalytic Activity of Metal-Organic Frameworks with Aminated-Functionalized Linkers: Substoichiometric Effects in MIL-125-NH2. *J. Am. Chem. Soc.* **2017**, *139* (24), 8222–8228. https://doi.org/10.1021/jacs.7b02186.
(22) Wang, J.; Cherevan, A. S.; Hannecart, C.; Naghdi, S.; Nandan, S. P.; Gupta, T.; Eder, D. Ti-Based MOFs: New Insights on the Impact of Ligand Composition and Hole Scavengers on Stability, Charge Separation and Photocatalytic Hydrogen Evolution. *Appl. Catal. B Environ.* **2021**, *283*. https://doi.org/10.1016/j.apcatb.2020.119626.
(23) Syzgantseva, M. A.; Stepanov, N. F.; Syzgantseva, O. A. Effect of Ligand Functionalization on the Rate of Charge Carrier Recombination in Metal-Organic Frameworks: A Case Study of MIL-125. *J. Phys. Chem. Lett.* **2021**, *12* (2), 829–834. https://doi.org/10.1021/acs.jpclett.0c03634.
(24) Hanna, L.; Long, C. L.; Zhang, X.; Lockard, J. V. Heterometal Incorporation in NH2-MIL-125(Ti) and Its Participation in the Photoinduced Charge-Separated Excited State. *Chem. Commun.* **2020**, *56* (78), 11597–11600. https://doi.org/10.1039/d0cc05339b.
(25) Li, L.; Cai, Z.; Wu, Q.; Lo, W.-Y.; Zhang, N.; Chen, L. X.; Yu, L. Rational Design of Porous Conjugated Polymers and Roles of Residual Palladium for Photocatalytic Hydrogen Production. *Journal of the American Chemical Society* **2016**, *138* (24), 7681.
(26) Du, X.-H.; Jiang, Z.; Liu, Z.; Xu, C., Assistant Professor. BODIPY-Linked Conjugated Porous Polymers for Dye Wastewater Treatment. *Microporous and Mesoporous Materials* **2022**, *332*. https://doi.org/10.1016/j.micromeso.2022.111711.
(27) Jaiswal, S.; Giri, A.; Mandal, D.; Sarkar, M.; Patra, A. UV-to-NIR Harvesting Conjugated Porous Polymer Nanocomposite: Upconversion and Plasmon Expedited Thioether Photooxidation. *Angewandte Chemie International Edition* **2023**, *62* (49), 1-1–12. https://doi.org/10.1002/anie.202312910.
(28) Chaoui, N.; Trunk, M.; Dawson, R.; Schmidt, J.; Thomas, A. Trends and Challenges for Microporous Polymers. *Chem. Soc. Rev.* **2017**, *46* (11), 3302–3321. https://doi.org/10.1039/c7cs00071e.
(29) Kolobov, N.; Goesten, M. G.; Gascon, J. Metal–Organic Frameworks: Molecules or Semiconductors in Photocatalysis? *Angew. Chem. - Int. Ed.* **2021**, *60* (50), 26038–26052. https://doi.org/10.1002/anie.202106342.
(30) Chambers, M. B.; Wang, X.; Elgrishi, N.; Hendon, C. H.; Walsh, A.; Bonnefoy, J.; Canivet, J.; Quadrelli, E. A.; Farrusseng, D.; Mellot-Draznieks, C.; Fontecave, M. Photocatalytic Carbon Dioxide Reduction with Rhodium-Based Catalysts in Solution and Heterogenized within Metal-Organic Frameworks. *ChemSusChem* **2015**, *8* (4), 603–608. https://doi.org/10.1002/cssc.201403345.

(31) Wisser, F. M.; Berruyer, P.; Cardenas, L.; Mohr, Y.; Quadrelli, E. A.; Lesage, A.; Farrusseng, D.; Canivet, J. Hammett Parameter in Microporous Solids as Macroligands for Heterogenized Photocatalysts. *ACS Catal.* **2018**, *8* (3), 1653–1661. https://doi.org/10.1021/acscatal.7b03998.
(32) Bloch, E. D.; Britt, D.; Lee, C.; Doonan, C. J.; Uribe-Romo, F. J.; Furukawa, H.; Long, J. R.; Yaghi, O. M. Metal Insertion in a Microporous Metal-Organic Framework Lined with 2,2'-Bipyridine. *J. Am. Chem. Soc.* **2010**, *132* (41), 14382–14384. https://doi.org/10.1021/ja106935d.
(33) Feng, X.; Ren, Y.; Jiang, H. Metal-Bipyridine/Phenanthroline-Functionalized Porous Crystalline Materials: Synthesis and Catalysis. *Coord. Chem. Rev.* **2021**, *438*. https://doi.org/10.1016/j.ccr.2021.213907.
(34) Ren, Z.; Liu, Y.; Lyu, Y.; Song, X.; Zheng, C.; Feng, S.; Jiang, Z.; Ding, Y. Single-Atom Rh Based Bipyridine Framework Porous Organic Polymer: A High Active and Superb Stable Catalyst for Heterogeneous Methanol Carbonylation. *J. Catal.* **2019**, *369*, 249–256. https://doi.org/10.1016/j.jcat.2018.11.015.
(35) Wisser, F. M.; Duguet, M.; Perrinet, Q.; Ghosh, A. C.; Alves-Favaro, M.; Mohr, Y.; Lorentz, C.; Quadrelli, E. A.; Palkovits, R.; Farrusseng, D.; Mellot-Draznieks, C.; de Waele, V.; Canivet, J. Molecular Porous Photosystems Tailored for Long-Term Photocatalytic CO2 Reduction. *Angew. Chem. - Int. Ed.* **2020**, *59* (13), 5116–5122. https://doi.org/10.1002/anie.201912883.
(36) Santaclara, J. G.; Nasalevich, M. A.; Castellanos, S.; Evers, W. H.; Spoor, F. C. M.; Rock, K.; Siebbeles, L. D. A.; Kapteijn, F.; Grozema, F.; Houtepen, A.; Gascon, J.; Hunger, J.; Van Der Veen, M. A. Organic Linker Defines the Excited-State Decay of Photocatalytic MIL-125(Ti)-Type Materials. *ChemSusChem* **2016**, *9* (4), 388–395. https://doi.org/10.1002/cssc.201501353.
(37) Constable, E. C.; Neuburger, M.; Rösel, P.; Schneider, G. E.; Zampese, J. A.; Housecroft, C. E.; Monti, F.; Armaroli, N.; Costa, R. D.; Ortí, E. Ligand-Based Charge-Transfer Luminescence in Ionic Cyclometalated Iridium(III) Complexes Bearing a Pyrene-Functionalized Bipyridine Ligand: A Joint Theoretical and Experimental Study. *Inorg. Chem.* **2013**, *52* (2), 885–897. https://doi.org/10.1021/ic302026f.
(38) Sprick, R. S.; Jiang, J.-X.; Bonillo, B.; Ren, S.; Ratvijitvech, T.; Guiglion, P.; Zwijnenburg, M. A.; Adams, D. J.; Cooper, A. I. Tunable Organic Photocatalysts for Visible-Light-Driven Hydrogen Evolution. *J. Am. Chem. Soc.* **2015**, *137* (9), 3265–3270. https://doi.org/10.1021/ja511552k.
(39) Ghose, A.; Rebarz, M.; Maltsev, O. V.; Hintermann, L.; Ruckebusch, C.; Fron, E.; Hofkens, J.; Mély, Y.; Naumov, P.; Sliwa, M.; Didier, P. Emission Properties of Oxyluciferin and Its Derivatives in Water: Revealing the Nature of the Emissive Species in Firefly Bioluminescence. *J. Phys. Chem. B* **2015**, *119* (6), 2638–2649. https://doi.org/10.1021/jp508905m.
(40) Bryckaert, M.; Kharchenko, A.; Lebedev, O.; Dong, B.; De Waele, I.; Buntinx, G.; Poizat, O.; Mintova, S.; De Waele, V. Hot-Electron Photodynamics of Silver-Containing Nanosized Zeolite Films Revealed by Transient Absorption Spectroscopy. *J. Phys. Chem. C* **2017**, *121* (48), 26958–26966. https://doi.org/10.1021/acs.jpcc.7b10727.
(41) Buntinx, G.; Naskrecki, R.; Poizat, O. Subpicosecond Transient Absorption Analysis of the Photophysics of 2,2'-Bipyridine and 4,4'-Bipyridine in Solution. *J. Phys. Chem.* **1996**, *100* (50), 19380–19388. https://doi.org/10.1021/jp960900v.
(42) Solé-Daura, A.; Benseghir, Y.; Ha-Thi, M.-H.; Fontecave, M.; Mialane, P.; Dolbecq, A.; Mellot-Draznieks, C. Origin of the Boosting Effect of Polyoxometalates in Photocatalysis: The Case of CO_2 Reduction by a Rh-Containing Metal–Organic Framework. *ACS Catal.* **2022**, *12* (15), 9244–9255. https://doi.org/10.1021/acscatal.2c02088.
(43) Pellegrin, Y.; Odobel, F. Sacrificial Electron Donor Reagents for Solar Fuel Production; [Les Donneurs d'électron Sacrificiels Pour La Production de Combustible Solaire]. *Comptes Rendus Chim.* **2017**, *20* (3), 283 – 295. https://doi.org/10.1016/j.crci.2015.11.026.
(44) Yamazaki, Y.; Takeda, H.; Ishitani, O. Photocatalytic Reduction of CO2 Using Metal Complexes. *J. Photochem. Photobiol. C Photochem. Rev.* **2015**, *25*, 106–137. https://doi.org/10.1016/j.jphotochemrev.2015.09.001.

(45) Sampaio, R. N.; Grills, D. C.; Polyansky, D. E.; Szalda, D. J.; Fujita, E. Unexpected Roles of Triethanolamine in the Photochemical Reduction of CO_2 to Formate by Ruthenium Complexes. *J. Am. Chem. Soc.* **2020**, *142* (5), 2413–2428. https://doi.org/10.1021/jacs.9b11897.
(46) Kim, S.; Ahn, D.-S.; Ahn, M.; Wee, K.-R.; Choi, J.; Ihee, H. Charge Transfer Induced by Electronic State Mixing in a Symmetric X–Y–X-Type Multi-Chromophore System. *Phys. Chem. Chem. Phys.* **2020**, *22* (48), 28440–28447. https://doi.org/10.1039/D0CP05132B.
(47) Weigel, W.; Rettig, W.; Dekhtyar, M.; Modrakowski, C.; Beinhoff, M.; Schlüter, A. D. Dual Fluorescence of Phenyl and Biphenyl Substituted Pyrene Derivatives. *J. Phys. Chem. A* **2003**, *107* (31), 5941–5947. https://doi.org/10.1021/jp026116u.
(48) Boilet, L.; Burdzinski, G.; Buntinx, G.; Lefumeux, C.; Poizat, O. Picosecond Absorption and Resonance Raman Investigation of the Dynamics of the Photoreduction of 4,4'-Bipyridine by Aliphatic Amines in Acetonitrile Solution. *J. Phys. Chem. A* **2001**, *105* (45), 10271–10277. https://doi.org/10.1021/jp010504z.
(49) Poizat, O.; Buntinx, G.; Boilet, L. Photoreduction of 4,4'-Bipyridine by Amines in Acetonitrile-Water Mixtures: Influence of H-Bonding on the Ion-Pair Structure and Dynamics. *J. Phys. Chem. A* **2005**, *109* (48), 10813–10823. https://doi.org/10.1021/jp058199v.
(50) Neuwahl, F. V. R.; Foggi, P. Direct Observation of S_2-S_1 Internal Conversion in Pyrene by Femtosecond Transient Absorption. *Laser Chem.* **1999**, *19* (1–4), 375–379. https://doi.org/10.1155/1999/37692.
(51) Raytchev, M.; Pandurski, E.; Buchvarov, I.; Modrakowski, C.; Fiebig, T. Bichromophoric Interactions and Time-Dependent Excited State Mixing in Pyrene Derivatives. A Femtosecond Broad-Band Pump−Probe Study. *J. Phys. Chem. A* **2003**, *107* (23), 4592–4600. https://doi.org/10.1021/jp027356c.
(52) Roos, M. K.; Reiter, S.; de Vivie-Riedle, R. Ultrafast Relaxation from 1La to 1Lb in Pyrene: A Theoretical Study. *Chem. Phys.* **2018**, *515*, 586–595. https://doi.org/10.1016/j.chemphys.2018.08.002.
(53) Fakis, M.; Beckwith, J. S.; Seintis, K.; Martinou, E.; Nançoz, C.; Karakostas, N.; Petsalakis, I.; Pistolis, G.; Vauthey, E. Energy Transfer and Charge Separation Dynamics in Photoexcited Pyrene-Bodipy Molecular Dyads. *Phys. Chem. Chem. Phys.* **2018**, *20* (2), 837–849. https://doi.org/10.1039/c7cp06914f.
(54) Patwardhan, S.; Jin, S.; Son, H.-J.; Schatz, G. C. Ultrafast Energy Migration in Porphyrin-Based Metal Organic Frameworks (MOFs); 2013; Vol. 1539, pp 22–27. https://doi.org/10.1557/opl.2013.987.
(55) Williams, D. E.; Shustova, N. B. Metal-Organic Frameworks as a Versatile Tool to Study and Model Energy Transfer Processes. *Chem. - Eur. J.* **2015**, *21* (44), 15474–15479. https://doi.org/10.1002/chem.201502334.
(56) Stanley, P. M.; Hemmer, K.; Hegelmann, M.; Schulz, A.; Park, M.; Elsner, M.; Cokoja, M.; Warnan, J. Topology- and Wavelength-Governed CO2 Reduction Photocatalysis in Molecular Catalyst-Metal-Organic Framework Assemblies. *Chem. Sci.* **2022**, *13* (41), 12164–12174. https://doi.org/10.1039/d2sc03097g.
(57) Gutiérrez-Arzaluz, L.; Jia, J.; Gu, C.; Czaban-Jóźwiak, J.; Yin, J.; Shekhah, O.; Bakr, O. M.; Eddaoudi, M.; Mohammed, O. F. Directional Exciton Migration in Benzoimidazole-Based Metal-Organic Frameworks. *J. Phys. Chem. Lett.* **2021**, *12* (20), 4917–4927. https://doi.org/10.1021/acs.jpclett.1c01053.
(58) Kent, C. A.; Mehl, B. P.; Ma, L.; Papanikolas, J. M.; Meyer, T. J.; Lin, W. Energy Transfer Dynamics in Metal-Organic Frameworks. *J. Am. Chem. Soc.* **2010**, *132* (37), 12767–12769. https://doi.org/10.1021/ja102804s.